Advanced Ceramics Progress: Vol. 10, No. 1, (Winter 2024) 1-10

Materials and Energy Research Center
MERC

Contents lists available at **ACERP**

Advanced Ceramics Progress

Journal Homepage: www.acerp.ir

Original Research Article

Gamma-ray Shielding Capacity of Ceramics Tb and Fe Doped with $Y_2Zr_2O_7$

Mohamadreza Alipoor [a], Mahdi Eshghi [b] *

[a] *PhD Candidate, Department t of Physics, Imam Hossein Comprehensive University, Tehran, Iran.*
[b] *Assistant Professor, Department t of Physics, Imam Hossein Comprehensive University, Tehran, Iran.*

* Corresponding Author Email: eshgi54@gmail.com. meshghi@ihu.ac.ir (Mahdi Eshghi)
URL: https://www.acerp.ir/article_206532.html

ARTICLE INFO

Article History:
Received: 03 December 2023
Revised: 06 April 2024
Accepted: 07 September 2024

Keywords:
Monte Carlo Simulations,
Gamma-ray Shielding,
Attenuation Coefficient,
Ceramics.

ABSTRACT

In this research, a Monte Carlo simulation was used to estimate the gamma-ray shielding properties of ceramics doped with Tb and Fe in $Y_2Zr_2O_7$, within the photon energy range of 0.015 to 15 MeV. We calculated the linear and mass attenuation coefficients, half-value layer, tenth-value layer, mean free path, effective atomic number, and fast neutron removal cross section. To validate the simulation, the results were compared with data obtained from the Phy-X program. It was observed that the data from the Phy-X program and the Geant 4 simulation tool were in good agreement. The ceramic sample YTF015, due to the addition of terbium, showed a significant increase in densification and microstructural development, leading to improved flexural strength and enhanced protection against fast neutrons and gamma radiation. The results indicate that energy levels significantly affect gamma-ray penetration. Furthermore, for the photon energy of 0.511 MeV, where the mass attenuation coefficient increased from 0.058 to 0.096 cm^2/g, YTF015 demonstrated superior shielding performance against gamma rays compared to other samples. In conclusion, YTF015 ceramics exhibited strong shielding properties, achieving 35% to 55% of the shielding capacity of pure lead element in the intermediate energy range of 0.1 to 2 MeV. This shows that the composition and microstructure of ceramic materials can be optimized to improve damping properties for applications in medical physics applications.

https://doi.org/10.30501/acp.2024.428521.1140

1. INTRODUCTION

Gamma rays are the most penetrating form of ionizing radiation and are widely used in medicine, including X-ray imaging and radiation therapy for cancer treatment. Other fields, such as nuclear power generation, also heavily rely on radiation. However, the growing range of radiation applications increases the risk of exposure to high-energy ionizing radiation (Asal & Erenturk, 2021). Ionizing radiation has been shown to cause permanent damage to both the human body and the environment, necessitating comprehensive preventive measures to mitigate these risks (Tekın at al., 2021). Radiation shielding materials must possess an adequate attenuation coefficient, strength, chemical stability, and temperature resistance (Alipoor & Eshghi, 2024, Hamad, 2023, Temir atal., 2021). Traditional radiation shields, such as lead and concrete, have limitations. Lead, despite its excellent attenuation properties, is unsuitable for long-term use in high-temperature environments due to its low melting point. Similarly, concrete suffers from damage such as cracking and flaking when exposed to radiation at high temperatures, which can impair its performance (Thiyagarajan at al., 2022, Han & Guo, 2017, Gu at al., 2022). As radiation shielding technology has evolved, various materials, including glasses, concretes, metal

Please cite this article as: Alipoor, M. & Eshghi, M. (2024). Gamma-ray Shielding Capacity of Ceramics Tb and Fe Doped with $Y_2Zr_2O_7$, *Advanced Ceramics Progress*, 10(1), 1-10. https://doi.org/10.30501/acp.2024.428521.1140

composites, and ceramics, have been explored for their potential use in shielding applications (Magnere at al., 2024, Ratep at al., 2024, Saleh at al., 2024, Naeema at al., 2024). For instance, composites are valued for their tunable structural properties but are less desirable for handling radioactive materials due to their poor heat transfer capabilities (Mahmoud at al., 2024, Ghule, 2024). Ceramics are a promising class of radiation shielding materials due to their ease of fabrication, durability, non-toxicity, and high melting points. These materials typically consist of non-metallic compounds (e.g., metal oxides, nitrides, carbides) combined with metallic elements, resulting in a crystalline or semi-crystalline structure (Alver at al., 2023, Madej at al., 2021). Over the past decades, ceramics and ceramic composites have been utilized in industry and medicine. Their high temperature resistance (>1200°C), conductivity, hardness, insulation properties, strong oxidation resistance, low thermal expansion, and low dielectric constant make them effective at shielding against gamma rays (Lakshminarayana at al., 2018, Aktaş at al., 2019, Kaçal at al., 2018). Recent studies have focused on improving the production and design of ceramics, as well as adjusting their phase and composition, expanding their potential applications (Khattari at al., 2024, Oto at al., 2019, Hannachi at al., 2023, Alhindawy at al., 2023, Rao at al., 2023). Doped zirconium ceramics have garnered significant attention for their excellent radiation shielding properties. Zirconium, known for its high hardness, wear resistance, and corrosion resistance, can be enhanced with rare earth elements (REEs) such as cerium, ytterbium, neodymium, and gadolinium. These dopants can impart desirable properties such as increased strength, electrical conductivity, and, importantly, enhanced radiation attenuation. REE-doped zirconia improves protective abilities by enhancing microstructure and density, making it effective at absorbing harmful photons due to its high atomic number and density. Additionally, REE-doped zirconia can reduce secondary radiation by capturing scattered electrons produced during absorption (Bawazeer at al., 2023, Okafor at al., 2021, Pantulap at al., 2023). Nickel-cobalt-boron (Ni-Co-B) doped boron nitride ceramics show excellent gamma-ray attenuation properties across various current densities. Investigations into the radiation shielding properties of Dufric ceramics with carbon nanotubes (CNTs) have shown that while CNTs can affect the network structure and unit cell shrinkage, their addition impacts the results (Du at al., 2013). Adding Y_2O_3 to ceramics, due to its high molecular mass, can enhance shielding properties, particularly against charged radiation and photons. Additionally, Y_2O_3 has a high neutron interaction cross-section (Alrowaili at al., 2023b).

In practice, the versatility and high stability of oxides combined with zirconium and yttrium elements are exceptional. These ceramics are also promising hosts due to their ability to incorporate a wide variety of dopants into their structure (Khan at al., 2023, Chan at al., 2023). Additionally, this structure is highly flexible; for example, the lattice can accommodate ionic replacements at all its crystal sites, as well as vacancies, which can enhance structural defects (Yao at al., 2022).

Considering the increasing need for radiation protection in various industries such as medicine and nuclear energy, zirconium ceramics doped with yttrium and terbium make it a suitable option for radiation protection applications. Also, the addition of these two elements, Yttrium and Terbium, can increase the neutron shielding of doped Zirconium ceramics and make it a suitable shield for use in radiation protection applications. Therefore, the currently investigated zirconium-doped ceramics can become a safe (lead-free), transparent, and robust alternative with high temperature resistance for radiation protection and control in hospitals, industries, and other areas where radiation is applied.

2. MATERIALS AND METHODS

To ensure better understanding, a theoretical background of common formulas for gamma radiation protection is given below. Then, the Geant4 simulation tool is briefly described.

2.1. Theory

The linear attenuation coefficient (μ) measuring the attenuation capacity (absorption + scattering) of the material against photon radiation is obtained using Formula 1 (Alipoor & Eshghi, 2024):

$$\mu = \frac{ln\left(\frac{I_0}{I}\right)}{x} \quad (1)$$

where the I and I_0 values are the photon intensities measured and x is the thickness of the irradiated material. The mass attenuation coefficient (μ_ρ, cm^2/g) is obtained from relation 2 by dividing μ by the specific weight of the material :

$$\mu_m = \sum_{i=1} W_i \left(\frac{\mu}{\rho}\right)_i \quad (2)$$

Half value of layer (HVL) and tenth value layer (TVL) are the thickness of the shield that reduced the half and the tenth of the incident radiation intensity, respectively, and these parameters can be calculated utilizing Equations 3 and 4 :

$$HVL(cm) = \frac{ln\,2}{\mu} = \frac{0.693}{\mu} \quad (3)$$

$$TVL(cm) = \frac{ln\,10}{\mu} = \frac{2.3026}{\mu} \quad (4)$$

The values of effective atomic number (Z_{eff}) and effective electron density (N_{eff}) of studied ceramics are determined by Equations 5 and 6 :

$$Z_{eff} = \frac{\sigma_a}{\sigma_e} \quad (5)$$

$$N_{eff}\left(electron/_{g}\right) = N_A \frac{nZ_{eff}}{A} = \frac{\mu_m}{\sigma_e} \quad (6)$$

The parameter Σ_R (removal cross-section) parameter could be explained as possibility of a fast neutron being removed from a group of high energetic uncollided neutrons after the first collision with the any substance. The value Σ_R for a multi-element material is calculated as follows (Alipoor & Eshghi, 2024):

$$\Sigma_R/\rho = \sum_i W_i \left(\Sigma_R/\rho\right) \quad (7)$$

2.2. Toolkit for the simulation Geant4

The mass attenuation coefficient for all ceramic samples was determined using the Geant4 Monte Carlo simulation, based on the geometry shown in Figure 1. Geant4 is an object-oriented simulation toolkit based on C++ and is widely used in various fields, including nuclear physics, medical physics, and high-energy physics. This simulation tool offers advanced options for defining elements, chemical compositions, and types of radiation (such as gamma rays and electrons) across a broad energy range, using a variety of comprehensive libraries.

Geant4 allows users to define materials (elements and compounds with different isotopes), create diverse detector geometries, generate particles and beams, and collect data on particle transport. The significance and validity of Geant4 simulations are discussed in references (Taheri at al., 2023). In this simulation, gamma photons were set with an energy spectrum ranging from 0.015 to 10 MeV. To achieve the desired outcome, several input files were created, including material, source, geometry, and detector information. The material was modeled as a blade with dimensions of 10×10×1 cm along the x, y, and z coordinates. Figure 1 shows a 3D view of the simulation, depicting a schematic representation of the narrow beam transmission geometry for gamma photons passing through the ceramic sample. In Figure 1, the green lines inside the blade represent the traces of gamma rays.

Photon attenuation was determined by simulating all possible physical processes affecting photons (such as photoelectric effects, Compton scattering, Rayleigh scattering, and pair production), as well as bremsstrahlung, ionization, and positron annihilation for electrons and positrons. These processes were simulated using physics models for electromagnetic processes available in G4EMStandardPhysics (options 1-4). These physics models are part of the Electromagnetics package, which utilizes evaluated data libraries to calculate time steps that model the interactions of photons and electrons with matter. To ensure accuracy, each simulation was performed with 10 million gamma photons and used option 4 of the electromagnetic physics models (Kelsey at al., 2023, Eshghi &Alipoor, 2024).

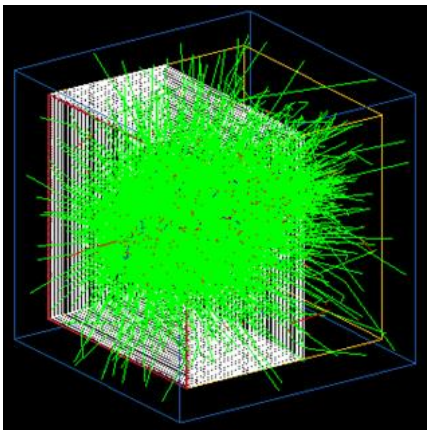

Figure 1. Schematic of configuration of shielding in Geant4 tool.

3. RESULTS AND DISCUSSION

In Table 1, five zirconium ceramics doped with Y and Fe are investigated for their gamma and neutron shielding properties (Jovaní at al., 2016).

TABLE 1. Chemical compounds of the selected ceramics.

Material	Density	%Weight Fractions				
		Y	Zr	Fe	O	Tb
YF015	5.42	0.5216	0.2676	0.1638	0.0419	--
YF025	4.6	0.4225	0.2167	0.1327	0.2281	--
YF035	4.74	0.4225	0.1167	0.2327	0.2281	--
YTF015	6.71	0.2164	0.222	0.1359	0.0389	0.3868
YTF025	5.8	0.1811	0.1858	0.1138	0.1956	0.3237
YTF035	5.94	0.1811	0.0858	0.2138	0.1956	0.3237

First, we calculated the mass attenuation coefficients using the Geant4 tool. Medical radiation is a branch of medicine that uses radiation to diagnose conditions such as bone fractures or tumors, and to treat these conditions. Diagnostic medical radiation typically ranges from approximately 0.015 to 0.5 MeV, while therapeutic medical radiation ranges from approximately 0.5 to 15 MeV. To illustrate the differences in shielding requirements for these energy ranges, we investigated both diagnostic and therapeutic energy fields in this study.

Mass attenuation coefficients were determined for each ceramic sample across a range of energies from 0.015 MeV to 15 MeV. In the next step, the same ceramic compounds (as listed in Table 1) were defined, including their densities, in the Phy-X/PSD program. Overall, the results obtained from the two programs were in good agreement with each other.

TABLE 2. Mass attenuation coefficients in terms of photon energy for the ceramics.

Energy (MeV)	YF015		YF025		YF035		YTF015		YTF025		YTF035	
	our work	Phy-X	our work	Phy-X	our work	Phy-X	our work	Phy-X	our work	Phy-X	our work	Phy-X
0.015	27.716	27.910	22.797	22.956	26.033	26.202	56.011	56.133	47.177	47.280	50.413	50.526
0.02	59.518	59.374	48.367	48.254	43.685	43.585	52.280	52.172	43.897	43.805	39.214	39.135
0.02634	28.616	28.665	23.266	23.307	20.945	20.968	25.122	25.136	21.103	21.115	18.782	18.776
0.04	9.248	9.206	7.539	7.506	6.756	6.730	8.150	8.154	6.863	6.866	6.080	6.090
0.0595	3.089	3.094	2.538	2.542	2.279	2.283	6.644	6.622	5.592	5.573	5.333	5.313
0.08	1.403	1.404	1.168	1.169	1.058	1.057	3.053	3.070	2.582	2.597	2.471	2.484
0.103	0.7416	0.743	0.6297	0.631	0.5751	0.577	1.598	1.600	1.363	1.364	1.308	1.309
0.15	0.3285	0.328	0.2917	0.291	0.2732	0.273	0.6428	0.639	0.5599	0.557	0.5414	0.539
0.284	0.1317	0.132	0.1273	0.128	0.1247	0.125	0.1863	0.187	0.1737	0.174	0.1710	0.172
0.364	0.1065	0.107	0.1051	0.105	0.1041	0.104	0.1343	0.135	0.1286	0.129	0.1275	0.128
0.4	0.0996	0.100	0.0989	0.099	0.0981	0.098	0.1213	0.121	0.1171	0.117	0.1163	0.116
0.511	0.0853	0.085	0.0856	0.085	0.0854	0.085	0.0964	0.096	0.0948	0.095	0.0946	0.094
0.662	0.0738	0.073	0.0745	0.074	0.0745	0.074	0.0791	0.079	0.0789	0.078	0.0789	0.078
0.723	0.0703	0.070	0.0711	0.071	0.0712	0.071	0.0745	0.074	0.0745	0.074	0.0746	0.074
0.826	0.0654	0.065	0.0664	0.066	0.0665	0.066	0.0682	0.068	0.0685	0.068	0.0687	0.068
1.1173	0.0542	0.054	0.0551	0.055	0.0553	0.055	0.0554	0.055	0.0556	0.055	0.0558	0.055
1.275	0.0519	0.051	0.0528	0.052	0.0531	0.053	0.0524	0.052	0.0531	0.053	0.0533	0.053
1.333	0.0507	0.050	0.0516	0.051	0.0517	0.051	0.0511	0.051	0.0518	0.052	0.052	0.052
1.5	0.0478	0.047	0.0485	0.048	0.0487	0.049	0.0481	0.048	0.0487	0.048	0.0489	0.049
2	0.0418	0.042	0.0423	0.042	0.0425	0.042	0.0423	0.042	0.0427	0.043	0.0428	0.043
3	0.0362	0.036	0.0361	0.036	0.0361	0.036	0.0373	0.037	0.0370	0.037	0.0370	0.037
4	0.0339	0.034	0.0334	0.033	0.0331	0.033	0.0355	0.036	0.0348	0.035	0.0346	0.035
5	0.0329	0.033	0.0319	0.032	0.0316	0.032	0.0351	0.035	0.0338	0.034	0.0336	0.034
6	0.0325	0.033	0.0312	0.031	0.0308	0.031	0.0352	0.035	0.0336	0.034	0.0334	0.033
8	0.0327	0.033	0.0308	0.031	0.0303	0.030	0.0361	0.036	0.0339	0.034	0.0335	0.034
10	0.0334	0.034	0.0310	0.031	0.0305	0.031	0.0374	0.038	0.0347	0.035	0.0342	0.034
15	0.0357	0.036	0.0324	0.033	0.03172	0.032	0.0407	0.041	0.0371	0.037	0.0364	0.037

However, many factors can affect the results of Monte Carlo simulations. Phy-X/PSD is a web-based tool that allows users to explore different shielding properties based on material definitions and energy ranges. Notably, the relative error between the outcomes of the two programs ranged from 0.84% to 0.09%. After verifying the compatibility of the simulation results, we calculated additional shielding parameters. The density and chemical composition of the manufactured ceramics are provided in Table 1. From this table, it is evident that the density of the ceramics increases with higher terbium concentration (Tb, Z=65), with the YTF015 sample showing the highest density value. According to Table 2, YTF015 exhibits the highest mass attenuation coefficients across the entire energy range, while YF025 shows the lowest coefficients.

From Figure 2, it was observed that there are peaks for the ceramics at photon energies of 17.03 and 17.99 keV. Since these photon energies fall within the region where the photoelectric absorption effect predominates, all ceramics exhibit the highest mass attenuation coefficients (μ) at these energies compared to other energy levels. These peaks correspond to the K-edge absorption of yttrium (at 17.0384 keV). As the energy increases, the probability of photoelectric absorption decreases, while the probability of Compton scattering increases. Consequently, the μ values decrease with increasing energy. Our findings clearly show that the YTF025 sample exhibits the highest values across all energies.

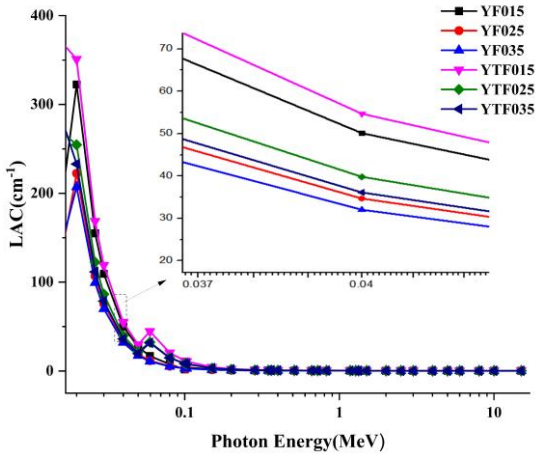

Figure 2. Linear attenuation coefficient (cm^{-1}) in terms of photon energy for ceramics.

It is important to note that the results were closely aligned due to variations in the incorporation of zirconium and terbium into the ceramics. However, the presence or absence of terbium had a substantial impact on the mass attenuation coefficients of the ceramics. Furthermore, as a density-independent parameter, the mass attenuation coefficient provides critical insights into the material's performance in relation to its elemental composition.

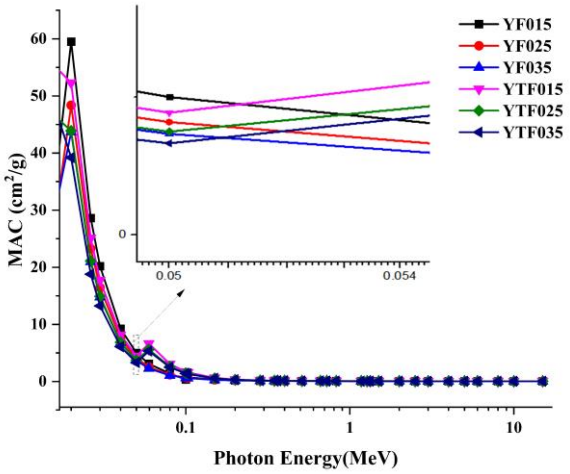

Figure 3. Mass attenuation coefficient(cm^2/g) in terms of photon energy for ceramics.

Meanwhile**,** Figure 3 clearly depicts the onset of the K-edge absorption peak for yttrium in the ceramics, as shown in magnification. This figure illustrates the variation of mass attenuation coefficients (μ_m) within the energy range from 0.15 to 15 MeV. Consistent with previous findings, the YTF015 sample exhibits the highest values. This observation can be partially attributed to the differing structural and atomic arrangements in YF015 and YTF015, which directly influence their gamma-ray attenuation properties.

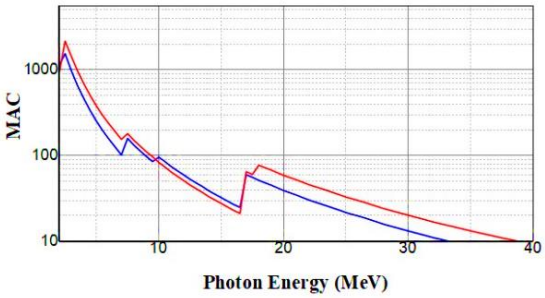

Figure 4. Mass attenuation coefficient (cm^2/g) in terms of photon energy for ceramics.

Figure 4 clearly illustrates the peaks associated with the photoelectric effect near the L2, L1, L3, and K edge absorptions of the yttrium element (at energies of 2.3725, 2.1555, 2.08, and 17.0384 keV, respectively), as well as the K edge absorption of the zirconium element (at an energy of 17.9976 keV). In addition, the L1 edge absorption of the terbium element is observed at 8.708 keV, extending up to 40 keV.

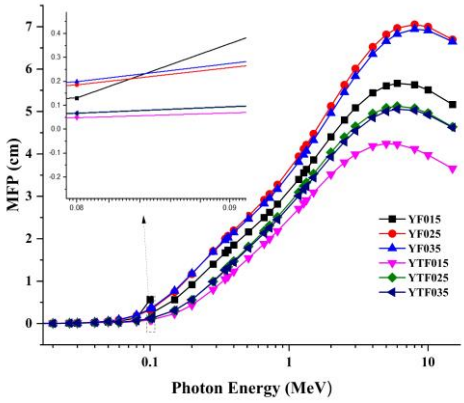

Figure 5. Mean free path(cm) in terms of photon energy for ceramics.

Another critical parameter for evaluating photon shielding characteristics is the mean free path (MFP), which represents the average distance a particle (photon, atom, or molecule) travels between two consecutive collisions. These collisions affect the particle's direction, energy, and other properties. The MFP is a crucial parameter that determines the effectiveness of radiation shielding. As depicted in Figure 5, the MFP is influenced by photon energy, with an increase in gamma photon energy leading to a longer MFP for the material. The changes in MFP are displayed over an energy range of 0.015 to 10 MeV. It is observed that, at lower energies below 1 MeV, the MFP increases slightly, while at energies above 1 MeV, the increase is more pronounced. Within the energy range of 0.1 to 1 MeV, the MFP increases almost uniformly. Notably, YF025 and YF035 exhibit higher MFP values compared to other materials, indicating that these materials interact less with photons and may not be ideal for shielding

applications. A significant increase in MFP is observed for the ceramic YF015 at an energy of 0.06 MeV (Figure 5).

The half-value layer (HVL) is another essential shielding parameter used to determine the specific thickness of an absorber required to reduce the photon intensity to 50% of its original value. A material with a lower HVL is generally more suitable for practical applications. Therefore, researchers aim to identify protective materials with relatively low HVL values. Figure 6 presents a graphical representation of the HVL data for the studied ceramics.

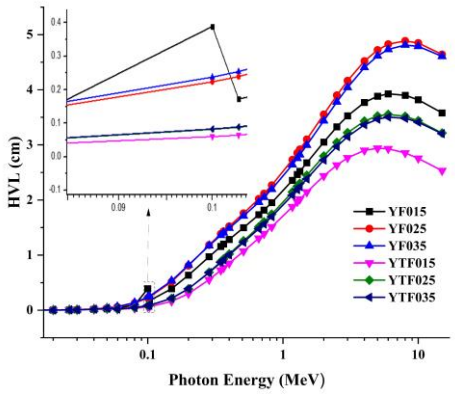

Figure 6. The half-value layer(cm) in terms of photon energy for ceramics.

The half-value layer (HVL) values exhibit a strong dependence on photon energy, increasing as the energy ranges from 0.1 to 10 MeV. The findings also indicate that HVL values are influenced by the composition and quantity of iron and terbium incorporated into the ceramics. Specifically, the results show that HVL is affected by the density of the material. Notably, the HVL for the YTF015 ceramic is lower compared to other ceramics. This observation suggests that an increase in the concentration of iron and terbium enhances the ability of the studied ceramics to attenuate photons.

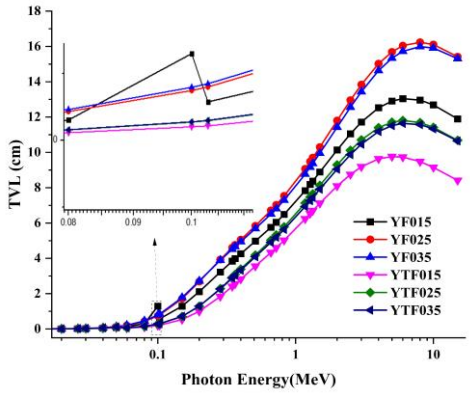

Figure 7. The tenth-value layer(cm) in terms of photon energy for ceramics.

In addition, another valuable parameter commonly used to estimate the attenuation effect of photons in various materials is illustrated in Figure 7. The tenth-value layers (TVLs) increase rapidly with energy, consistent with findings from studies analyzing TVL for the ceramics under investigation. In other words, the results for TVL closely match those for the half-value layer (HVL) reported previously. Our results indicate that the YTF015 sample, with the highest terbium (Tb) content, exhibits the lowest TVL values across all energy levels.

For instance, at an energy of 0.511 MeV, the TVL values for the samples were reported as 4.976 cm, 5.844 cm, 5.685 cm, 3.555 cm, 4.183 cm, and 4.095 cm for YF015, YF025, YF035, YTF015, YTF025, and YTF035, respectively. Both TVL and HVL values vary with increasing iron and terbium content and with the increasing density of the studied ceramics.

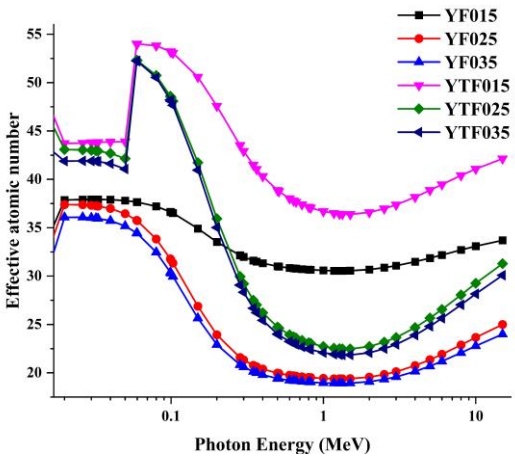

Figure 8. The effective atomic number, Z_{eff}, in terms of photon energy for ceramics.

The concept of effective atomic number (Z_{eff}) is employed to characterize the electromagnetic interaction of gamma ray photons with a compound. This parameter considers both the atomic composition and the density of the material. Z_{eff} is defined as a calculated value representing the average atomic numbers of the constituent elements, adjusted for their respective electron densities. An increased Z_{eff} value indicates a higher frequency of scattering interactions, thereby enhancing the material's effectiveness in scattering low-energy gamma rays. At higher energy levels, the significance of Z_{eff} diminishes, with other factors, particularly the nuclear properties of the shielding materials and their role in pair production interactions, becoming more relevant. Thus, a thorough analysis of shielding material selection, considering gamma ray energy and specific interaction processes, is essential for optimizing shielding performance. Figure 8 illustrates the variations in Z_{eff} values for the studied ceramics across different gamma ray energies. The YTF015

sample consistently exhibits the highest effective atomic number (Z_{eff}) values at all energy levels, which may be attributed to its superior gamma ray absorption capabilities.

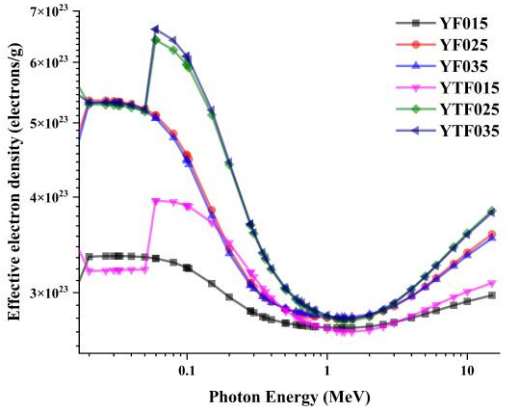

Figure 9. The effective electron density, N_{eff}, in terms of photon energy for ceramics.

Figure 9 displays the dependence of electron density, N_{eff}, values on photon energy across the range of 0.015 to 10 MeV for all samples. It is evident from the figure that fluctuations in N_{eff} are significant, mirroring the trends observed for the effective atomic number Z_{eff}. These trends are also influenced by the average atomic mass (A), where Z represents the number of protons or electrons in each sample.

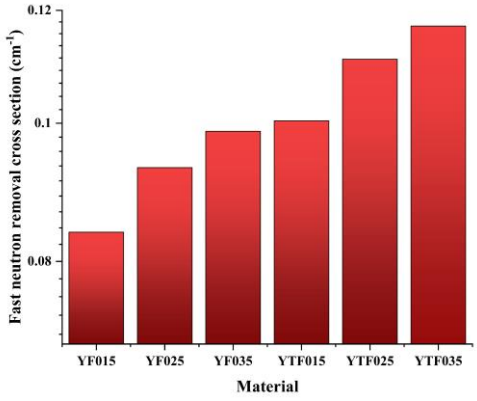

Figure 10. Fast neutron removal cross section (cm^{-1}) with photon energy for ceramics.

The effective fast neutron removal cross-section (Σ_R) is shown in Figure 10 for all samples using bar representation in units of cm^{-1}. The calculated Σ_R for all studied ceramics shows that YTF035 has the highest value (Σ_R = 0.117), indicating the fact that the effective removal cross-section of fast neutrons increases with decreasing zirconium percentage. On the contrary, the lowest calculated Σ_R = 0.083 is for sample YF015 with the most zirconium. These related variations of Σ_R with respect to physical and mechanical properties may suggest a way to design ceramic composites that can meet the engineering and shielding requirements of gamma and neutron radiation for specific applications. Depending on the shielding parameters considered, it may be possible to determine the best shielding parameter for a particular application.

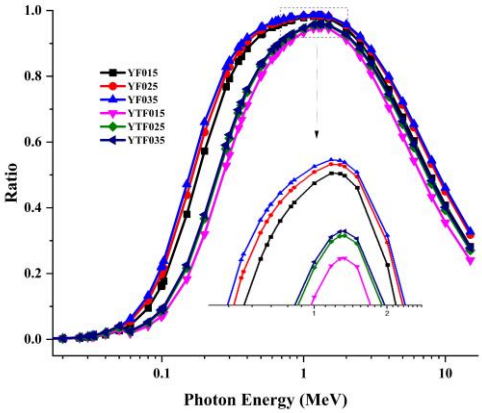

Figure 11. The $Ratios\ (\mu_m)_{Compton} / (\mu_m)_{total}$ with photon energy for ceramics.

Further, variation of ratios $(\mu_m)_{Compton} / (\mu_m)_{total}$ versus the energy photon (0.015–10 MeV) is presented for ceramics in Figure 11. The value of $(\mu_m)_{Compton}/(\mu_m)_{total}$ at ~1000 keV belongs to the maximum value of $(\mu_m)_{Compton} / (\mu_m)_{total}$. This figure clearly illustrates that as photon energy increases and Compton scattering becomes more dominant, the radiation absorption performance decreases. According to Figure 11, YTF015 ceramic exhibits favorable characteristics for radiation protection, demonstrating a lower absorption-to-scattering ratio compared to other samples.

- Buildup factors play a crucial role in the design of effective radiation shields. This study aimed to quantify the energy absorption exposure buildup factor (EBF) values for the ceramics under investigation, considering various mean free path parameters. Figures 10 and 11 demonstrate that the relative EBF values tend to be higher for stable nuclei under low-energy conditions. This observation suggests that stable nuclei are held together by strong forces, requiring significant energy input to destabilize them. Conversely, light nuclei may exhibit lower EBF values, yet they still indicate a bound state.
- At intermediate energy levels, EBF values can remain significantly high, although they are more sensitive to the specific reaction mechanisms involved. Certain reactions may have increased likelihoods and enhanced energetic favorability, leading to alterations in nuclear characteristics. This variability explains why the photoelectric effect and transitions are prominent in low and high-energy regions. In these processes, photons are either fully

absorbed or significantly reduced, resulting in less accumulation.

- At moderate energies, Compton scattering predominates, causing photons to scatter rather than being completely absorbed. This scattering also leads to multiple photon interactions, which affects the EBF. As the proportion of zirconium (Zr) decreases, energy absorption in YF ceramics diminishes, particularly noticeable in the 50 to 100 keV energy range. Moreover, a decrease in the percentage of terbium (Tb) leads to a reduction in energy absorption in YFT ceramics. This effect is particularly noticeable at energies below 100 keV.

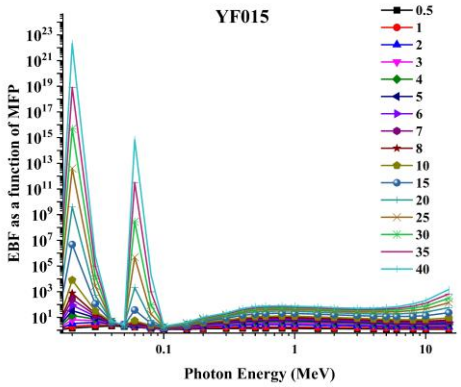

Figure 12-a. Variation of exposure buildup factor (EBF) with photon energy at different mean free paths for ceramics.

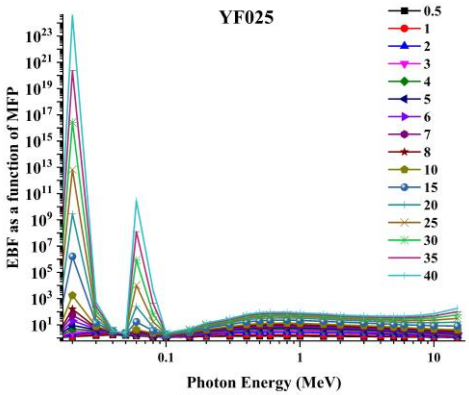

Figure 12-b. Variation of exposure buildup factor (EBF) with photon energy at different mean free paths for ceramics.

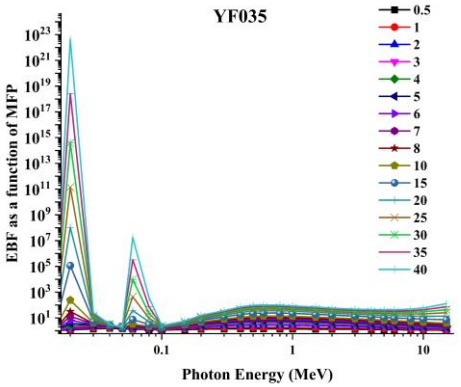

Figure 12-c. Variation of exposure buildup factor (EBF) with photon energy at different mean free paths for ceramics.

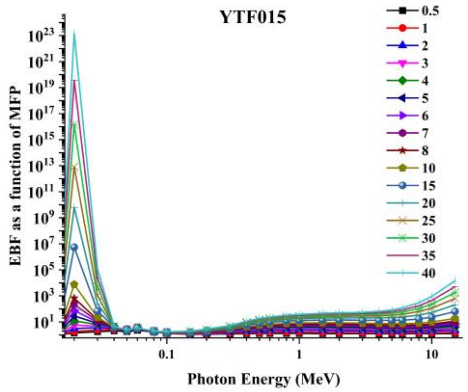

Figure 12-d. Variation of exposure buildup factor (EBF) with photon energy at different mean free paths for ceramics.

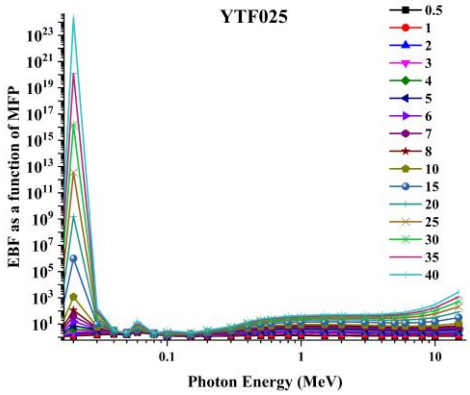

Figure 12-e. Variation of exposure buildup factor (EBF) with photon energy at different mean free paths for ceramics.

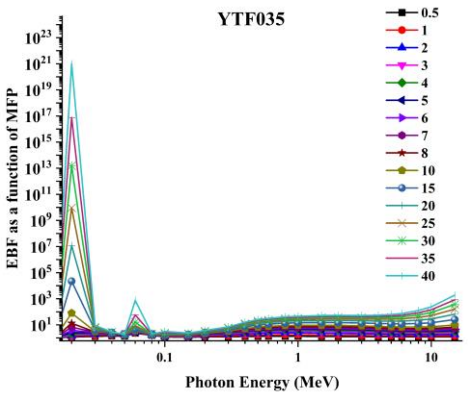

Figure 12-f. Variation of exposure buildup factor (EBF) with photon energy at different mean free paths for ceramics.

4. CONCLUSION

In this study, we examined the shielding properties of ceramics against ionizing radiation, including linear attenuation coefficient, mass attenuation coefficient, half-value layer, tenth-value layer, and mean free path (MFP) across a photon energy range of 0.015 to 15 MeV, using the Geant4 and Phy-X programs, which produced consistent results. The findings indicated that the YTF015 ceramic, enhanced with terbium, showed notable improvements in densification, microstructural development, and flexural strength, leading to increased protection against fast neutron and gamma radiation. The study also demonstrated that energy levels significantly impact gamma ray penetration, with YTF015 exhibiting strong shielding performance at 0.511 MeV, where the mass attenuation coefficient dropped from 0.58 to 0.096 cm. Compared to pure lead, YTF015 ceramics offered effective shielding, achieving 35% to 55% of pure lead's shielding capacity in the 0.1 to 2 MeV energy range, highlighting the potential of ceramic materials' composition and microstructure in optimizing attenuation properties for medical physics applications.

ACKNOWLEDGEMENTS

Thanks to the dear referees who helped improve the quality of the article. Also, we appreciate and thank all the magazine officials for the good editing of the proof of the article.

REFERENCES

1. Aktas, B., Yalcin, S., Dogru, K., Uzunoglu, Z., & Yilmaz, D. (2018). Structural and radiation shielding properties of chromium oxide doped borosilicate glass. *Radiation Physics and Chemistry*, 156, 144–149. https://doi.org/10.1016/j.radphyschem.2018.11.012
2. Alipoor, M. R., & Eshghi, M. (2024). Nickel/Multiwalled carbon nanotube composites as Gamma-Ray shielding. *NANO*, 19(06). https://doi.org/10.1142/s1793292024500279
3. Alipoor, M., & Eshghi, M. (2024). Monte Carlo simulation and determination of gamma ray protection characteristics of composites containing Bismuth Oxide and elements of Gadolinium, Titanium, Tungsten, Zirconium, Zinc and Yttrium. *Journal of Science and Technology of Composites*, 10(4), 2348-2356. https://doi.org/10.22068/jstc.2024.2007267.1845
4. Alipoor, M., & Eshghi, M. (2024). Shielding properties of iron-doped nano-hydroxides against gamma-rays. *Journal of Nuclear Science, Engineering and Technology (JONSAT)*, 45(4). https://doi.org/10.24200/nst.2024.1643
5. Alhindawy, I. G., Sayyed, M., Aloraini, D. A., Almuqrin, A. H., Alomar, M. S., Elawadi, G. A., & Mahmoud, K. (2024). A multi-phase investigation to understand the function of lanthanum and neodymium in the zirconia ceramics' synthesis, structural, and gamma-ray protective ability. *Radiation Physics and Chemistry*, 215, 111336. https://doi.org/10.1016/j.radphyschem.2023.111336
6. Alrowaili, Z., Kırkbınar, M., İbrahimoğlu, E., Çalışkan, F., Alruwaili, N. S., Elhadi, M., Al-Buriahi. (2023b). Radiation shielding performance of recycled waste CRT glasses doped with Li_2O and Y_2O_3: Potential applications in medical facilitates. *Radiation Physics and Chemistry*, 212, 111200. https://doi.org/10.1016/j.radphyschem.2023.111200
7. Alver, Ü., Duran, S. U., Demirköz, M., Muçogllava, B., Aslan, M., Çava, K., Dindar, O. (2023). Ulexite/HDPE-Bi2O3/HDPE layered composites for neutron and gamma radiation shielding. *Applied Radiation and Isotopes*, 200, 110940. https://doi.org/10.1016/j.apradiso.2023.110940
8. Asal, S., Erenturk, S. A., & Haciyakupoglu, S. (2020). Bentonite based ceramic materials from a perspective of gamma-ray shielding: Preparation, characterization and performance evaluation. *Nuclear Engineering and Technology*, 53(5), 1634–1641. https://doi.org/10.1016/j.net.2020.11.009
9. Bawazeer, O., Makkawi, K., Aga, Z. B., Albakri, H., Assiri, N., Althagafy, K., & Ajlouni, A. (2023). A review on using nanocomposites as shielding materials against ionizing radiation. *Journal of Umm Al-Qura University for Applied Sciences*, 9(3), 325–340. https://doi.org/10.1007/s43994-023-00042-9
10. Chen, Y., Zhang, R., Hu, S., Jiang, P., Sun, J., Zhang, B., & Zhang, Y. (2022). Mechanical properties of (ZrYTaErTi)O composites. *Ceramics International*, 49(3), 5261–5268. https://doi.org/10.1016/j.ceramint.2022.10.044
11. Du, Q., Zhou, G., Zhou, J., Jia, X., & Zhou, H. (2012). Enhanced luminescence of novel $Y_2Zr_2O_7:Dy^{3+}$ phosphors by Li_+ co-doping. *Journal of Alloys and Compounds*, 552, 152–156. https://doi.org/10.1016/j.jallcom.2012.10.074
12. Eshghi, M., & Alipoor, M. (2024). A Comprehensive Study of Gamma-rays Shielding Features of Binary Compounds. *Progress in Physics of Applied Materials*, 4(1), 59-67. https://doi.org/10.22075/ppam.2024.32949.1082
13. Ghule, P. G., Bholane, G., Joshi, R., Dahiwale, S., Shelke, P., & Dhole, S. (2023). Gamma radiation shielding properties of unsaturated polyester /Bi_2O_3 composites: An experimental, theoretical and simulation approach. *Radiation Physics and Chemistry*, 216, 111452. https://doi.org/10.1016/j.radphyschem.2023.111452
14. Gu, Y., Wang, J., Wang, Y., Xu, C., Liu, Y., Du, L., Liu, Q. (2022). Low-dose ionizing radiation exposure and risk of leukemia: results from 1950–1995 Chinese medical X-ray workers' cohort study and meta-analysis. *Journal of the National Cancer Center*, 2(2), 90–97. https://doi.org/10.1016/j.jncc.2022.01.001
15. Hamad, M. K. (2023). Effects of bismuth substitution on the structural and ionizing radiation shielding properties of the novel BaSnBiO perovskites: An experimental study. *Materials Chemistry and Physics*, 308, 128254. https://doi.org/10.1016/j.matchemphys.2023.128254
16. Han, J., & Guo, G. (2017). Characteristics of energy deposition from 1-1000 MeV proton and neutron induced nuclear reactions in silicon. *AIP Advances*, 7(11). https://doi.org/10.1063/1.4995529
17. Hannachi, E., Sayyed, M., Slimani, Y., Almessiere, M., Baykal, A., & Elsafi, M. (2023). Experimental study on the radiation protecting ability of composites containing barium titanate and nanospinel ferrite. *Radiation Physics and Chemistry*, 212, 111126. https://doi.org/10.1016/j.radphyschem.2023.111126
18. Jovaní, M., Sanz, A., Beltrán-Mir, H., & Cordoncillo, E. (2016). New red-shade environmental-friendly multifunctional pigment based on Tb and Fe doped $Y_2Zr_2O_7$ for ceramic applications and cool roof coatings. *Dyes and Pigments*, 133, 33–40. https://doi.org/10.1016/j.dyepig.2016.05.042
19. Kacal, M. R., Akman, F., & Sayyed, M. I. (2018). Investigation of radiation shielding properties for some ceramics. *Radiochimica Acta*, 107(2), 179–191. https://doi.org/10.1515/ract-2018-3030

20. Kelsey, M., Agnese, R., Alam, Y., Langroudy, I. A., Azadbakht, E., Brandt, D., Zatschler, S. (2023). G4CMP: Condensed matter physics simulation using the Geant4 toolkit. *Nuclear Instruments and Methods in Physics Research Section a Accelerators Spectrometers Detectors and Associated Equipment*, 1055, 168473. https://doi.org/10.1016/j.nima.2023.168473

21. Khan, M. Z., Gul, I. H., Javaid, F., Ali, A., Hafeez, S., & Baig, M. M. (2023). Synthesis and characterization of Zr^{4+}-Y^{3+} substituted BA-SR hexaferrite nanoparticles for microwave absorption and electromagnetic shielding applications. *Materials Research Bulletin*, 168, 112468. https://doi.org/10.1016/j.materresbull.2023.112468

22. Khattari, Z. Y., Zakaly, H. M. H., Alrowaily, A. W., Ene, A., Shams, M. S., Issa, S. a. M., Rammah, Y. S. (2023). A comprehensive study on optical, physical, mechanical and radiation shielding properties of calcium bismuth borophosphate glass–ceramics with distinct V_2O_5 contents. *Optical and Quantum Electronics*, 56(1). https://doi.org/10.1007/s11082-023-05598-8

23. Lakshminarayana, G., Baki, S., Sayyed, M., Dong, M., Lira, A., Noor, A., Mahdi, M. (2017). Vibrational, thermal features, and photon attenuation coefficients evaluation for TeO_2-B_2O_3-BaO-ZnO-Na_2O-Er_2O_3-Pr_6O_{11} glasses as gamma-rays shielding materials. *Journal of Non-Crystalline Solids*, 481, 568–578. https://doi.org/10.1016/j.jnoncrysol.2017.11.049

24. Madej, D., Silarski, M., & Parzych, S. (2020). Design, structure, microstructure and gamma radiation shielding properties of refractory concrete materials containing Ba- and Sr-doped cements. *Materials Chemistry and Physics*, 260, 124095. https://doi.org/10.1016/j.matchemphys.2020.124095

25. Magnere, S. M., Toledo, E. A., Yazdani-Pedram, M., Fuentealba, P., Contreras-Soto, A., Bascuñan-Heredia, A., Aguilar-Bolados, H. (2024). High performance fluoroelastomer composites filled with graphite and/or bismuth oxide for applications in gamma-ray shielding. *Polymer Composites*. https://doi.org/10.1002/pc.28237

26. Mahmoud, K., Binmujlli, M., Marashdeh, M., Sayyed, M., Aljaafreh, M. J., Akhdar, H., & Alhindawy, I. G. (2024). Comprehensive analysis of the effects of Mo and Co on the synthesis, structural, and radiation-shielding properties of TiO_2 based composites. *Progress in Nuclear Energy*, 169, 105105. https://doi.org/10.1016/j.pnucene.2024.105105

27. Naeema, N., Kadhim, O. J., Abdullah, N. J., Aldhuhaibat, M. J., Bakhtiar, H., & Salim, A. (2024). Shielding performance of metal oxide nanoparticles-doped polypropylene composites against gamma rays and neutrons exposure. *Radiation Physics and Chemistry*, 216, 111461. https://doi.org/10.1016/j.radphyschem.2023.111461

28. Okafor, C. E., Okonkwo, U. C., & Okokpujie, I. P. (2021). Trends in reinforced composite design for ionizing radiation shielding applications: a review. *Journal of Materials Science*, 56(20), 11631–11655. https://doi.org/10.1007/s10853-021-06037-3

29. Oto, B., Kavaz, E., Durak, H., Aras, A., & Madak, Z. (2019). Effect of addition of molybdenum on photon and fast neutron radiation shielding properties in ceramics. *Ceramics International*, 45(17), 23681–23689. https://doi.org/10.1016/j.ceramint.2019.08.082

30. Pantulap, U., Arango-Ospina, M., & Boccaccini, A. R. (2021). Bioactive glasses incorporating less-common ions to improve biological and physical properties. *Journal of Materials Science Materials in Medicine*, 33(1). https://doi.org/10.1007/s10856-021-06626-3

31. Rao, L. S., Hussain, S., Navalika, A., & Hila, F. C. (2024). Morphology, structural, and radiation shielding characteristics of Bi_2O_3-B_2O_3-Cr_2O_3: ZrO_2 glass ceramics. *Ceramics International*, 50(6), 9811–9819. https://doi.org/10.1016/j.ceramint.2023.12.302

32. Ratep, A., Abdelaziem, A., Hanfi, M. Y., Mahmoud, K. A., & Kashif, I. (2023). Enhancing gamma-ray shielding with bismuth oxide-infused boron oxides. *Optical and Quantum Electronics*, 56(2). https://doi.org/10.1007/s11082-023-05788-4

33. Saleh, A., Almohiy, H., Shalaby, R. M., & Saad, M. (2023). Comprehensive investigation on physical, structural, mechanical and nuclear shielding features against X/gamma-rays, neutron, proton and alpha particles of various binary alloys. *Radiation Physics and Chemistry*, 216, 111443. https://doi.org/10.1016/j.radphyschem.2023.111443

34. Taheri, A., Khandaker, M. U., Moradi, F., & Bradley, D. A. (2023). A review of recent advances in the modeling of nanoparticle radiosensitization with the Geant4-DNA toolkit. *Radiation Physics and Chemistry*, 212, 111146. https://doi.org/10.1016/j.radphyschem.2023.111146

35. Tekin, H. O., Bilal, G., Zakaly, H. M. H., Kilic, G., Issa, S. a. M., Ahmed, E. M., & Ene, A. (2021). Newly developed Vanadium-Based glasses and their potential for nuclear radiation shielding aims: A Monte Carlo Study on gamma ray attenuation parameters. *Materials*, 14(14), 3897. https://doi.org/10.3390/ma14143897

36. Temir, A., Zhumadilov, K., Zdorovets, M., Kozlovskiy, A., & Trukhanov, A. (2021). Study of gamma radiation shielding efficiency with radiation-resistant Bi_2O_3-TeO_2-WO_3 ceramics. *Solid State Sciences*, 115, 106604. https://doi.org/10.1016/j.solidstatesciences.2021.106604

37. Thiyagarajan, G. B., Koroleva, E., Filimonov, A., Vakhrushev, S., & Kumar, R. (2021). Thermally tunable dielectric performance of t-ZrO_2 stabilized amorphous Si(Pb,Zr)OC ceramic nanocomposites. *Materials Chemistry and Physics*, 277, 125495. https://doi.org/10.1016/j.matchemphys.2021.125495

38. Yao, Y., Ren, G., Yu, Y., Che, J., Liang, T., Li, L., . . . Zhao, X. (2022). Thermal conduction mechanism of ferroelastic Zr-Y-Yb-Ta-Nb-O high-entropy oxides with glass-like thermal conductivity. Journal of the American Ceramic Society, 105(6), 4360–4374. https://doi.org/10.1111/jace.18374